BNL-228463-2025-TECH

EIC-ADD-TN-128

Ring Electron Cooler for Electron Ion Collider

S. Seletskiy

July 2025

Electron-Ion Collider

Brookhaven National Laboratory

U.S. Department of Energy

USDOE Office of Science (SC), Nuclear Physics (NP)

DISCLAIMER

Ring Electron Cooler for Electron Ion Collider

S. Seletskiy*, J. Kewisch†, Y. Jing, A. Fedotov, D. Kayran
Brookhaven National Laboratory

J. Unger‡, G. Hoffstaetter
Cornell University

July 11, 2025

Contents

*seletskiy@bnl.gov
†jorg@bnl.gov
‡jeu8@cornell.edu

Abstract

This is a brief summary of feasibility studies of the Ring Electron Cooler (REC) for the Electron Ion Collider (EIC).

1 Introduction

Cooling of protons at top energy ($\gamma = 293$) to counteract the IBS-driven emittance growth can be beneficial to the EIC performance. The Ring Electron Cooler provides such capability.

The REC utilizes a well-established technique of regular electron cooling [1, 2].

In the REC, the hadrons are cooled with non-magnetized electron bunches. Such an approach was successfully applied at the Low Energy RHIC Electron Cooler [3, 4, 5, 6, 7, 8] during RHIC operation in 2019-2021 runs.

The electron bunches, used in the REC, are stored in a dedicated electron storage ring for several seconds. Thus, the same e-bunches are reused for the cooling on multiple turns. The electrons' emittances are preserved during the storage cycle by counteracting heating caused by various scattering mechanisms with radiation damping facilitated by dedicated damping wigglers.

2 REC design parameters

The main design parameters of the Ring Electron Cooler are listed in Tables 1 and 2. The cooler with the listed parameters provides cooling times of 2 hours in horizontal and 3 hours in longitudinal directions, which is adequate for compensating the IBS.

Table 1: The REC parameters (electron storage ring)

relativistic γ	293
ring circumference [m]	426
cooling section length [m]	170
horizontal dispersion in the CS [m]	1
number of damping wigglers	18
damping wiggler length [m]	4.2
damping wiggler field [T]	2.4
wiggler gap [cm]	2
wiggler period [cm]	23
momentum compaction	$-1.5 \cdot 10^{-3}$
main RF frequency [MHz]	98.6
main RF voltage [kV]	50
2nd harmonic RF voltage [kV]	25
number of bunches	140
number of particles per bunch	$1.3 \cdot 10^{11}$
charge per bunch [nC]	21
peak current [A] (flat top e-bunch)	17.5
average current [A]	2
geometric emittance (x, y) [nm]	7.8, 7.8
CS β-function (x, y) [m]	180, 160
rms relative momentum spread	$9.8 \cdot 10^{-4}$
FWHM bunch length (flat top e-bunch) [cm]	34
space charge tune shift (x,y)	0.14, 0.14
p-e focusing tune shift (x,y)	0.04, 0.09
radiation damping rate (x,y,z) [s^{-1}]	31, 31, 62
BBS rate (x,y,z) [s^{-1}]	0.8, -0.3, 12
IBS rate (x,y,z) [s^{-1}]	31, 31, 48

Table 2: The REC parameters (protons in the cooling section)

relativistic γ	293
number of particles per bunch	$6.9 \cdot 10^{10}$
geometric emittance (x, y) [nm]	11.3, 1
CS β-function (x, y) [m]	300, 700
rms relative momentum spread	$6 \cdot 10^{-4}$
rms bunch length (Gaussian p-bunch) [cm]	6
horizontal dispersion in the CS [m]	2.1
cooling time (x,y,z) [hrs]	**2, 4, 3**

3 Optimal cooling

3.1 Cooling rates in non-magnetized electron cooling

The cooling rates ($\lambda_{x,y,z} \equiv \frac{1}{\varepsilon_{x,y,z}} \frac{\varepsilon_{x,y,z}}{dt}$) in a non-magnetized bunched cooler, in the presence of electrons' and hadrons' dispersions in the cooling section, and assuming the Maxwell-Boltzmann velocity distributions for both beams, are given by [9, 10]:

$$
\begin{aligned}
\lambda_x &= -\frac{A_0}{\sigma_x\sigma_y\sigma_z}(\Psi_x + \kappa\Psi_z) \\
\lambda_y &= -\frac{A_0}{\sigma_x\sigma_y\sigma_z}\Psi_y \\
\lambda_z &= -\frac{A_0}{\sigma_x\sigma_y\sigma_z}(\Psi_z - \kappa\Psi_z)
\end{aligned}
$$

$$
A_0 = \frac{4\sqrt{2}}{\pi} c r_e r_i \frac{\eta N_e \Lambda_C}{\gamma^2\beta^3}
$$

$$
\kappa = \frac{D_{ex}D_{ix}\sigma_{\delta e}^2 + D_{ix}^2\sigma_{\delta i}^2}{\sigma_{xe}^2 + D_{ex}^2\sigma_{\delta e}^2 + \sigma_{xi}^2 + D_{ix}^2\sigma_{\delta i}^2}
$$

$$
\begin{aligned}
\Psi_x &= \int_0^\infty \frac{p^2 dp}{\left(1+2p^2\gamma^2\sigma_{\theta x}^2\right)^{3/2}\sqrt{1+2p^2\gamma^2\sigma_{\theta y}^2}\sqrt{1+2p^2\sigma_\delta^2}} \\
\Psi_y &= \int_0^\infty \frac{p^2 dp}{\sqrt{1+2p^2\gamma^2\sigma_{\theta x}^2}\left(1+2p^2\gamma^2\sigma_{\theta y}^2\right)^{3/2}\sqrt{1+2p^2\sigma_\delta^2}} \\
\Psi_z &= \int_0^\infty \frac{p^2 dp}{\sqrt{1+2p^2\gamma^2\sigma_{\theta x}^2}\sqrt{1+2p^2\gamma^2\sigma_{\theta y}^2}\left(1+2p^2\sigma_\delta^2\right)^{3/2}}
\end{aligned}
\tag{1}
$$

$$
\begin{aligned}
\sigma_x &= \sqrt{\sigma_{xe}^2 + D_{ex}^2\sigma_{\delta e}^2 + \sigma_{xi}^2 + D_{ix}^2\sigma_{\delta i}^2} \\
\sigma_y &= \sqrt{\sigma_{ye}^2 + \sigma_{yi}^2} \\
\sigma_z &= \sqrt{\sigma_{ze}^2 + \sigma_{zi}^2} \\
\sigma_{\theta x} &= \sqrt{\sigma_{\theta xe}^2 + \sigma_{\theta xi}^2} \\
\sigma_{\theta y} &= \sqrt{\sigma_{\theta ye}^2 + \sigma_{\theta yi}^2} \\
\sigma_\delta &= \sqrt{\sigma_{\delta e}^2 + \sigma_{\delta i}^2 - \frac{\left(D_{ex}\sigma_{\delta e}^2 + D_{ix}\sigma_{\delta i}^2\right)^2}{\sigma_{xe}^2 + D_{ex}^2\sigma_{\delta e}^2 + \sigma_{xi}^2 + D_{ix}^2\sigma_{\delta i}^2}}
\end{aligned}
$$

where N_e is number of electrons per bunch, r_e and r_i are electron and ion classical radii respectively, c is the speed of light, Λ_C is the Coulomb logarithm, γ is the relativistic gamma factor, $\eta = L_{CS}/C_R$, L_{CS} is a cooling section (CS) length and C_R is a circumference of an ion storage ring, D_{ex} and D_{ix} are horizontal dispersions in the CS for electrons and ions respectively, $\sigma_{(xe,ye,ze)}$ and $\sigma_{(xi,yi,zi)}$ are the respective rms sizes of the e- and i- bunches, $\sigma_{(\theta xe,\theta ye)}$ and $\sigma_{(\theta xi,\theta yi)}$ are

bunches' angular spreads, and $\sigma_{\delta e}$ and $\sigma_{\delta i}$ are the rms relative energy spreads of the electron and ion bunches respectively.

If e-bunch has a flat-top longitudinal distribution approximated by

$$f_{ze}(z) = \begin{cases} \frac{1}{L_{ze}}, & -\frac{L_{ze}}{2} \leq z \leq \frac{L_{ze}}{2} \\ 0, & z < -\frac{L_{ze}}{2} \cup z > \frac{L_{ze}}{2} \end{cases} \tag{2}$$

then, σ_z in Eq. (1) must be substituted with:

$$\sigma_z = \frac{\sqrt{2\pi}}{L_{ze}} \mathrm{erf}\left(\frac{L_{ze}}{2\sqrt{2}\sigma_{zi}}\right) \tag{3}$$

3.2 Optimization of cooling section parameters

Electron bunch parameters in the REC are determined by an interplay of several effects: the intra-beam scattering (IBS) of electrons, the beam-beam scattering (BBS) of electrons on hadrons in the cooling section, the quantum excitations (although it is a very small effect for the REC parameters), and the radiation damping of electrons' emittances and energy spread facilitated by the REC damping wigglers. The equilibrium x, y-emittances and energy spread are achieved when the damping rate (λ_{damp}) becomes equal to the overall heating rate characterized by the IBS rate (λ_{IBS}), the BBS rate (λ_{BBS}), and the rate quantum excitations ($\lambda_{damp}\varepsilon_{nat}$, where ε_{nat} is a natural emittance):

$$\frac{d\varepsilon}{dt} = (-\lambda_{damp} + \lambda_{IBS} + \lambda_{BBS})\varepsilon + \lambda_{damp}\varepsilon_{nat} \tag{4}$$

A dedicated code based on solving Eq. (4) was created to find equilibrium electron beam parameters. The Bjorken-Mtingwa IBS model with horizontal and vertical dispersion is used in the code [11]. The code also uses fast algorithm for IBS calculation [12].

A theoretical model of beam-beam scattering in the cooling section was developed [13], to be used in the code. Details of BBS calculations will be discussed in Section 5.1.

The radiation damping is mostly provided by the damping wigglers. This topic will be discussed in Section 4.4.1.

The overall optimization of the REC parameters is an iterative multi-step process involving (but not limited to):

- Choosing wiggler's field profile, which strongly affects dynamic and momentum apertures
- Solving Eq. (4) for equilibrium e-bunch parameters

- Choosing cooling section parameters, which affects cooling rate, proton-electron beam-beam effect, beam-beam scattering
- Checking resulting cooling rates along with collective effects and beam lifetime
- Optimizing the dynamic and momentum apertures and adjusting the REC lattice

An example of one of the steps on a final iteration of optimization of the CS parameters is demonstrated in Fig. 1. In this example the electron bunch β-functions and horizontal dispersion in the CS were kept constant, the longitudinal cooling time was kept at $\tau_z = 3$ hours and for each combination of ions β-functions (β_{xi}, β_{yi}) the horizontal cooling time was minimized by varying ions' horizontal dispersion (D_i) in the CS.

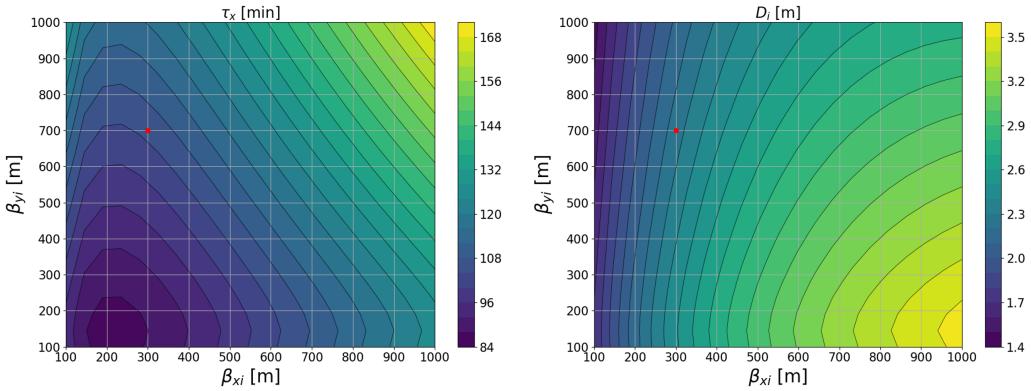

Figure 1: Optimization of protons parameters in the REC cooling section.

After each iteration the BBS rate was checked and the equilibrium e-beam parameters were recalculated. Furthermore, the beam-beam effect was simulated for the chosen parameters to check its effect on electrons' emittance.

The red dot in Fig. 1 shows the choice of protons Twiss parameters which maximize the cooling rate while keeping tolerable BBS rate and proton-electron beam-beam effect. The beam-beam effect will be discussed in more details in Section 5.3.

4 Ring Electron Cooler layout, optics and subsystems

4.1 REC location and layout

The Ring Electron Cooler must be located in the "2 o'clock interaction region" (IR2) of the Hadron Storage Ring (HSR), as Fig. 2 shows.

The REC will share the cooling section with the EIC Low Energy Cooler (LEC). Therefore, the REC lattice was designed in such a way that the REC cooling section would be compatible with the LEC.

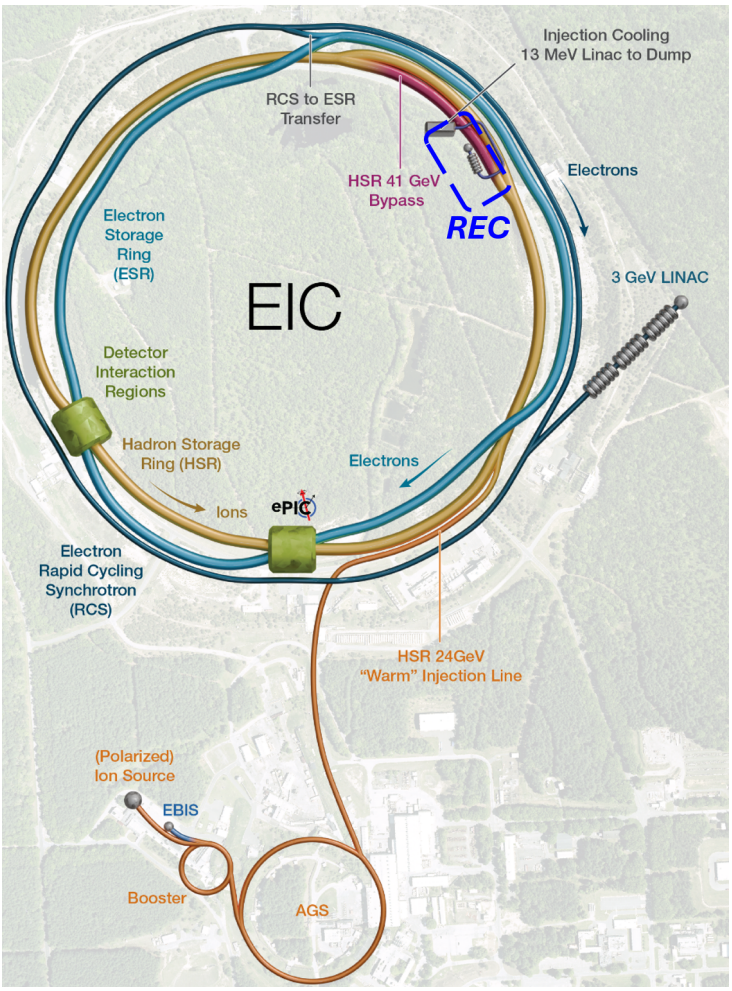

Figure 2: Schematics of the EIC layout.

The layout of the REC is shown in Fig. 3.

The 170 m long REC cooling section is a drift shielded by several

layers of μ-metal. The shielding will provide an attenuation factor of at least 1000, which will suppress the ambient field below 0.5 mG. The BPMs and correctors (both dipole correctors for e-beam trajectory, and solenoids for possible focusing correction) will be located every 12 m throughout the CS.

Opposite to the cooling section there is a wiggler section containing 18 damping wigglers. The wigglers must provide enough radiation cooling of the electron bunches to counteract the effects of the IBS and BBS.

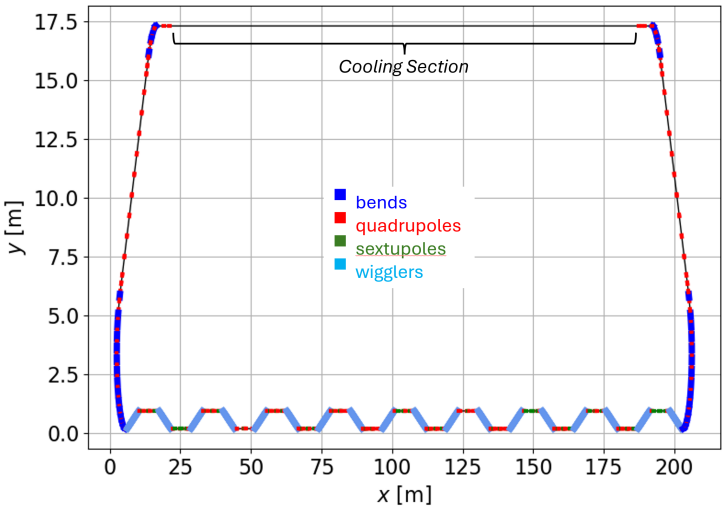

Figure 3: Schematics of the REC layout.

4.2 REC lattice

The REC lattice is shown in Fig. 4.

The matching sections at the entrance and the exit of the REC cooling section produce Twiss parameters needed for optimal cooling (see Fig. 5).

The wigglers are inclined with respect to the axis of the wiggling section with an angle alternating in sign from wiggler to wiggler. This design produces substantial dispersion in the regions between the wigglers (see Fig. 6), which allows to place sextupoles controlling the REC chromaticity inside the wiggler section.

The horizontal β-function is tightly focused inside the wigglers. Since the wigglers have small D_x and large D'_x, keeping β_x small allows to minimize an $\mathcal{H}$-function inside the wigglers, thus minimizing the IBS-driven emittance growth in the wiggler section.

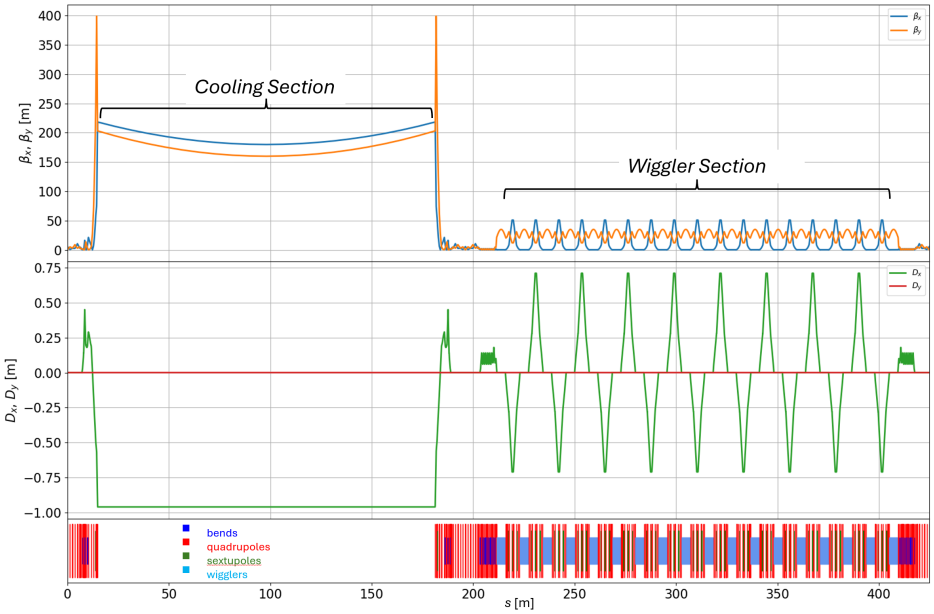

Figure 4: The Ring Electron Cooler lattice.

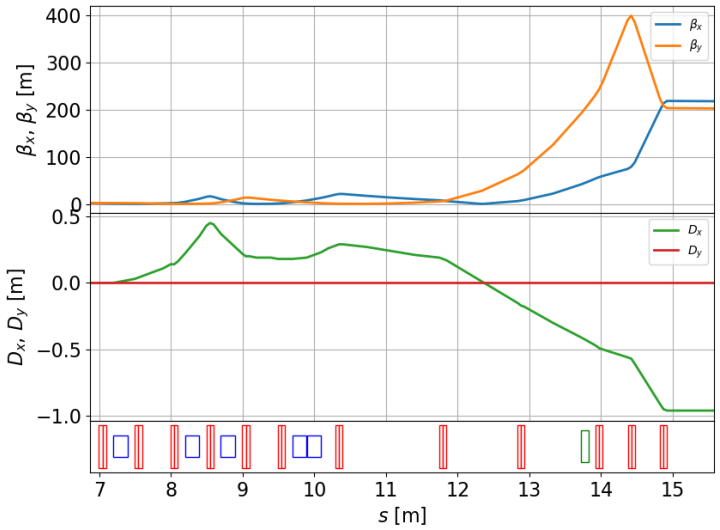

Figure 5: Matching section at the entrance to the REC CS.

The wigglers' design will be discussed in more details in Section 4.4.1.

The arcs connecting the CS and the wiggler section contain straight dispersion-less sections reserved for the RF (see Section 4.4.3) and injection (see Section 4.4.2) systems.

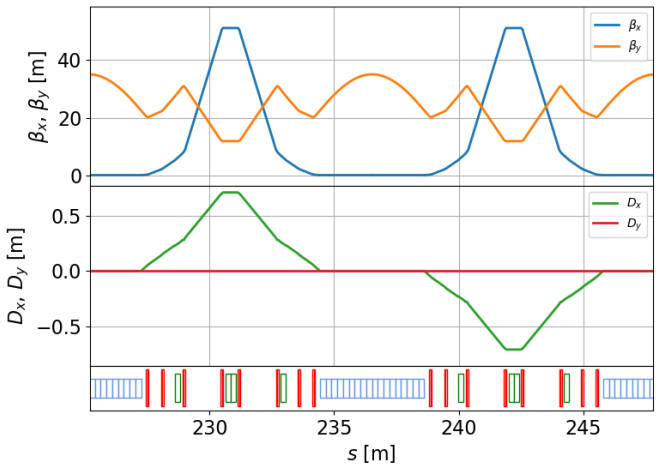

Figure 6: Wiggler section.

4.3 Dynamic and momentum apertures

Optimization of dynamic and momentum apertures (DA and MA) was an iterative multi-step process.

One of the most important steps in controlling the REC chromaticity and maximizing the momentum aperture was choosing the proper field profile for the wigglers (see Section 4.4.1 for more details).

To fine-tune a phase advance over the "wiggler-sextupoles blocks", which maximizes the DA , an automated algorithm was devised and used.

An addition of two families of octupoles reducing the nonlinear motion further improved the dynamic aperture.

The final step in DA/MA optimization was adjusting the betatron tunes.

The dynamic and momentum apertures of $A_x = 10\sigma_x$, $A_y = 9\sigma_y$ and $A_\delta = 0.5\%$ were achieved (see Fig. 7).

4.4 REC subsystems

In this section we consider several of the REC subsystems in more details.

4.4.1 Damping wigglers

The REC wiggler section contains $N_w = 18$ damping wigglers, $L_w = 4.2$ m long each. The peak field of a wiggler is $B_w = 2.4$ T. The

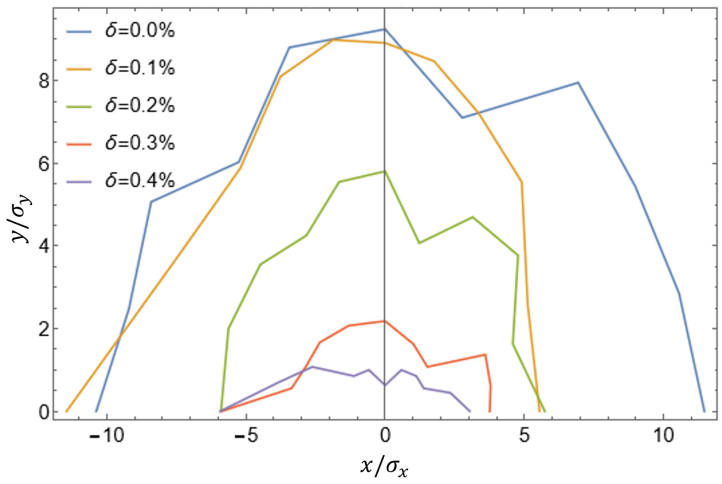

Figure 7: Dynamic aperture at various relative momenta.

resulting damping time (for amplitudes) is:

$$\tau_{damp(z)} = \frac{\tau_{damp(x,y)}}{2} = \frac{E}{U_{loss}} T_{rev} \tag{5}$$

where electrons' energy $E = 149$ MeV, the REC's revolution period $T_{rev} = C_{ring}/(\beta c) = 1.42$ μs, $C_{ring} = 426$ m being the REC circumference, and

$$\begin{aligned} U_{loss}[\text{MeV}] &= \frac{C_\gamma}{2\pi} E^4 I_{2w} = \frac{C_\gamma}{2\pi} E^4 \frac{B_w^2 \cdot N_w L_w}{2(B\rho)^2} = \\ &= 6.34 \cdot 10^{-10} (E[\text{MeV}])^2 \cdot (B_w[\text{T}])^2 \cdot N_w L_w[\text{m}] \end{aligned} \tag{6}$$

Equations (5) and (6) give the radiation cooling rates for emittances $\lambda_{dampW(x,y)} = 2/\tau_{damp(x,y)} = 58\ \text{s}^{-1}$ and $\lambda_{dampW(z)} = 2/\tau_{damp(z)} = 29\ \text{s}^{-1}$. The overall radiation cooling in the REC, taking into account the damping due to bending magnets, is $\lambda_{dampREC(x,y)} = 31\ \text{s}^{-1}$ and $\lambda_{dampREC(z)} = 62\ \text{s}^{-1}$. Such a damping allows to compensate the IBS, BBS and quantum excitations effects, and keeps electron bunch emittances at $\varepsilon_{x,y} = 7.8$ nm and its energy spread at $\sigma_{\delta e} = 9.8 \cdot 10^{-4}$.

The REC utilizes high field wigglers at a relatively low energy and small $\beta_x \approx 30$ cm throughout the wiggler, as discussed in Section 4. To satisfy these requirements while limiting the wigglers' contribution to the REC chromaticity [14], one must make magnetic field in the wigglers close to the field given by:

$$\begin{aligned} B_x &= \tfrac{k_x}{k_y} B_w \sinh(k_x x) \sinh(k_y y) \sin(kz) \\ B_y &= B_w \cosh(k_x x) \cosh(k_y y) \sin(kz) \\ B_z &= \tfrac{k}{k_y} B_w \cosh(k_x x) \sinh(k_y y) \cos(kz) \end{aligned} \tag{7}$$

where $k = 2\pi/\lambda$, and geometric parameters k_x and k_y are related via $k_x^2 + k_y^2 = k^2$.

Formulas (7) represent a wiggler with the poles shaped to produce a parabolic dependence of B_y on x near the center of the wiggler. Thus, the additional focusing in the x direction is happening due to a bunch going with an offset through a sextupole-like field.

Such a wiggler behaves as a thick lens. The matched beta-functions in a wiggler are given by:

$$\beta_x = \frac{\sqrt{2}kB\rho}{B_w k_x}; \quad \beta_y = \frac{\sqrt{2}kB\rho}{B_w\sqrt{k^2 - k_x^2}} \tag{8}$$

The resulting chromaticities are given by:

$$\begin{aligned} \eta_x &= -\tfrac{1}{2\pi}\tfrac{B_w L_w}{\sqrt{2}B\rho}\tfrac{k_x}{k} \\ \eta_y &= -\tfrac{1}{2\pi}\tfrac{B_w L_w \lambda}{\sqrt{2}B\rho}\tfrac{\sqrt{k^2-k_x^2}}{k} \end{aligned} \tag{9}$$

The optimized wiggler's parameters are listed in Table 3.

Table 3: REC wigglers' parameters

peak field (B_0) [T]	2.38
wiggler period (λ_w) [m]	0.23279
number of periods (N_p)	18
magnetic gap [mm]	21.8
wave number $k = 2\pi/\lambda$ [m^{-1}]	26.990787
k_x [m^{-1}]	26.990786
$k_y = \sqrt{k^2 - k_x^2}$ [m^{-1}]	0.00737
matched horizontal β-function (β_x) [m]	0.295
horizontal chromaticity η_x	-2.26
vertical chromaticity η_y	$-6 \cdot 10^6 - 4$

The wigglers with required field profile can be produced by utilizing permanent magnet poles with proper Vanadium Permendur shims. The conceptual design of such wigglers was created [15].

4.4.2 Injection system

The REC will have a top-off injection with a pulsed septum delivering the injected beam to the storage ring and a four-bump fast kick moving the stored beam closer to the injected one and then bringing both beams to the design orbit. The injection section setup is schematically

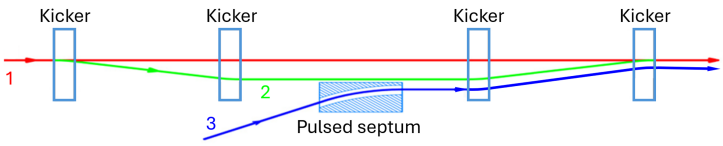

Figure 8: Schematic layout of injection section: 1 - undisturbed stored beam, 2- stored beam affected by an injection 4-bump kick, 3- injected beam. The overall length of the injection section is 2.5 m.

Table 4: Injection magnets parameters

parameter	Kicker	Septum
maximum field [G]	760	7000
magnetic length [m]	0.2	≥ 0.38
pulse shape	trapezoid	full sin-wave
rise/fall time [ns]	200	N/A
flat-top duration [ns]	284	N/A
wavelength [μs]	N/A	200
repetition rate [Hz]	3-5	3-5

shown in Fig. 8. The parameters of the injection magnets are listed in Table 4.

The Twiss parameters of the injected and the stored beams in the injection section and the emittance of the injected bunches must allow fitting both beams into an acceptance determined by the dynamic aperture of the ring (see Section 4.3). Figure 9 shows horizontal phase space of of the two beams and Table 5 lists respective parameters of the beams.

Table 5: Beam parameters in the injection section

parameter	stored bunch	injected bunch
horizontal β-function [m]	60	20
geometric horizontal emittance [nm]	8	5
normalized emittance in the injector [μm]	N/A	1.5
bunch charge [nC]	21	1.75

The time structure of the injection scheme is determined by the beam lifetime, which in the REC case is defined by the elastic scattering and is equal to 16.2 s (see Section 5.4).

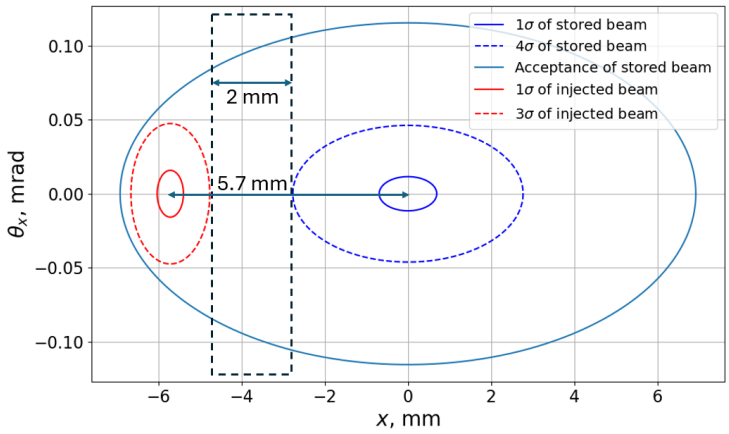

Figure 9: Horizontal phase space of the stored and injected beams. The stored beam is deflected towards the septum by the 4-bump kick.

The top-off injection will be done into 1/5 of the ring with an injection frequency $f_{inj} = 3$ Hz. The initial injection shall be performed with $f_{inj0} = 5$ Hz. Therefore, the injector must provide trains of 100 MHz 28 bunches (train length 0.284 μs) repeated with f_{inj} or f_{inj0}.

The intensity of a single bunch during the initial injection is shown in Fig. 10.

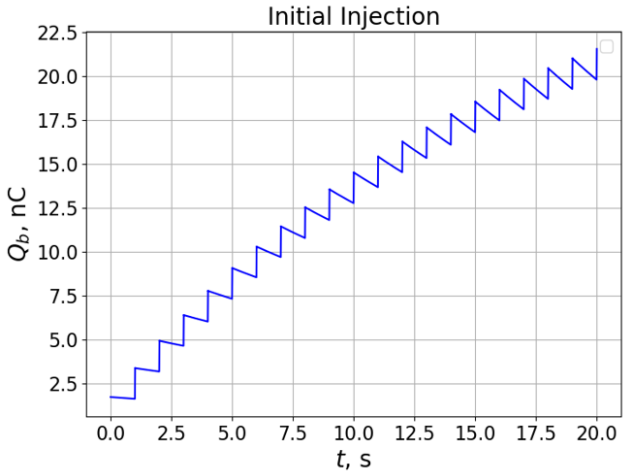

Figure 10: Feeling a bucket during initial injection.

The suggested top-off injection scheme will keep the average cooling rate at 96% of the peak value. The evolution of the cooling rate during the store is shown in Fig. 11.

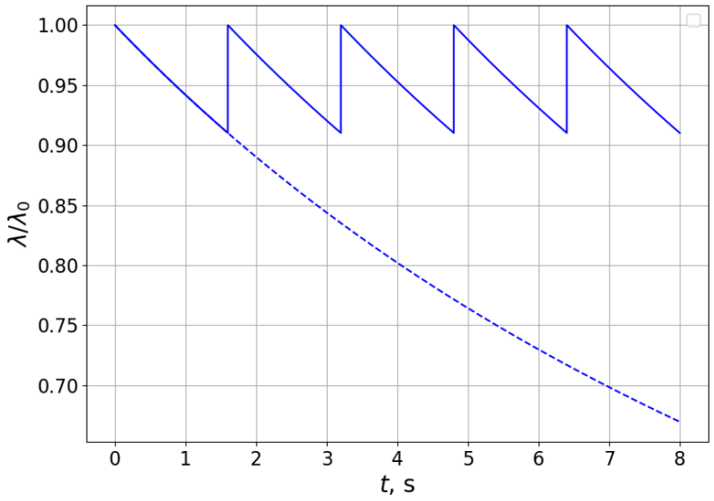

Figure 11: Cooling rate during the store.

4.4.3 RF system

The REC employs a double RF system to reduce the e-bunch peak current and limit the space charge effects (see Section **??**). The main parameters of the RF system and the resulting relevant e-bunch parameters are listed in Table 6.

Table 6: RF system parameters

parameter	value
main RF frequency [MHz]	98.6
main RF voltage [kV]	50
main RF phase [degrees]	7.24
radiation loss compensated by RF [kV/turn]	6
2nd harmonic RF voltage [kV]	25
number of particles per bunch	$1.3 \cdot 10^{11}$
charge per bunch [nC]	21
peak current [A] (flat top e-bunch)	17.5
rms relative momentum spread	$9.8 \cdot 10^{-4}$
FWHM bunch length (flat top e-bunch) [cm]	34

The individual components of the momentum kick on an electron stored in the REC are shown in Fig. 12. The resulting RF bucket is shown in Fig. 13.

We simulate the resulting electron bunch by injecting the Gaussian

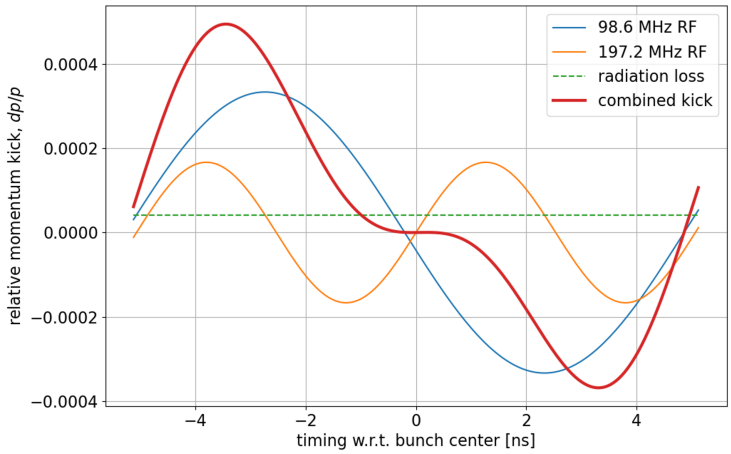

Figure 12: Relative momentum kick vs. electron's timing w.r.t. central particle.

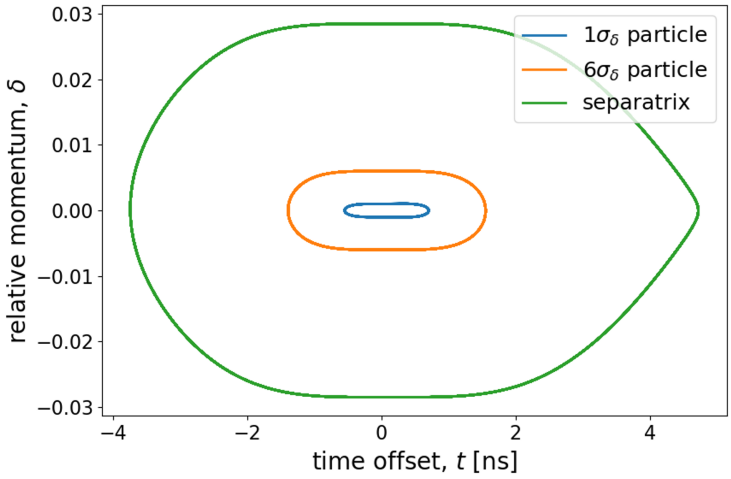

Figure 13: The REC RF bucket.

e-bunch with $\sigma_t = 0.3$ ns and $\sigma_\delta = 9 \cdot 10^{-4}$ into the bucket shown in Fig 13 and letting the bunch evolve for 50000 turns. The longitudinal profile of the REC bunch is shown in Fig. 14

5 Beam dynamics

5.1 Beam-beam scattering

Similar to the intra-beam scattering, in the REC cooling section the electrons are getting scattered on the ions. This process of beam-beam

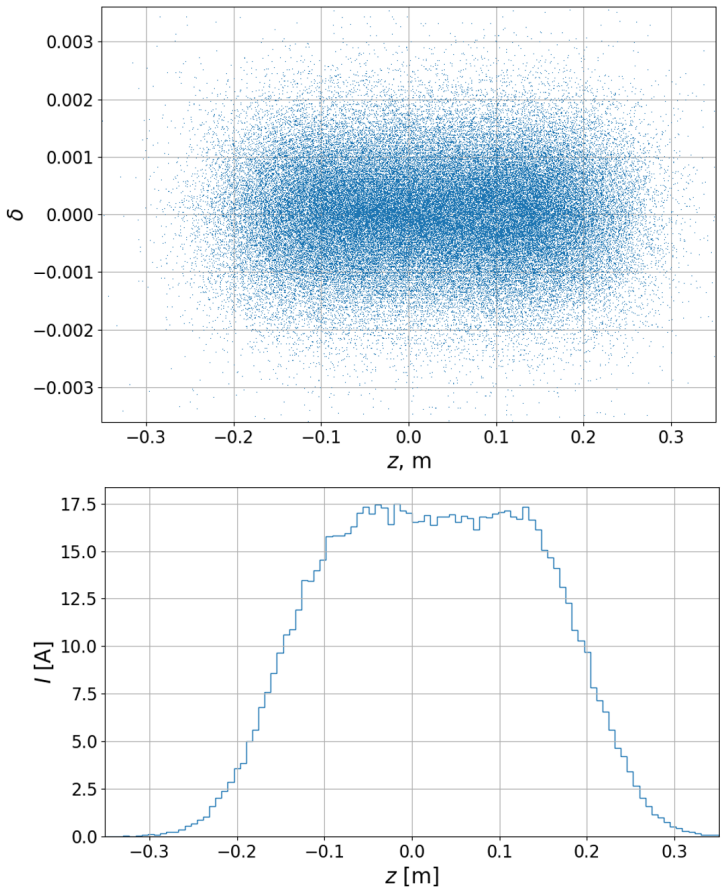

Figure 14: Electron bunch in the REC RF bucket.

scattering (BBS) leads to diffusive growth of e-bunches' emittance and energy spread. The theoretical model describing this process was developed [13]. Here, we give the explicit formulas for calculating the BBS effect.

The BBS-driven emittance growth rate is given by:

$$\lambda_{x,y,z} = \mathcal{C}_{x,y,z}\Psi_{x,y,z} \tag{10}$$

The coefficients $\mathcal{C}_{x,y,z}$ are given by:

$$\begin{aligned} \mathcal{C}_x &= \frac{r_e^2 Z_i^2 c^4 \Lambda_C n_i \eta}{2\pi^2 \gamma \Delta_{ix}\Delta_{iy}\Delta_{iz}\Delta_{ex}^3\Delta_{ey}\Delta_{ez}} \\ \mathcal{C}_y &= \frac{r_e^2 Z_i^2 c^4 \Lambda_C n_i \eta}{2\pi^2 \gamma \Delta_{ix}\Delta_{iy}\Delta_{iz}\Delta_{ex}\Delta_{ey}^3\Delta_{ez}} \\ \mathcal{C}_z &= \frac{r_e^2 Z_i^2 c^4 \Lambda_C n_i \eta}{2\pi^2 \gamma \Delta_{ix}\Delta_{iy}\Delta_{iz}\Delta_{ex}\Delta_{ey}\Delta_{ez}^3} \end{aligned} \tag{11}$$

where, r_e is the classical radius of electron, Z_i is the ion charge number,

c is the speed of light, Λ_C is the Coulomb logarithm, n_i is the ion bunch density in the beam frame, $\eta = L_{CS}/C_R$ is the duty factor, and the rms velocity spreads of electron and ion beams in the beam frame are denoted as $\Delta_{ex,ey,ez}$ and $\Delta_{ix,iy,iz}$ respectively.

The functions $\Psi_{x,y,z}$ are the 3D integrals given by:

$$\begin{aligned}
\Psi_x &= \int d^3u \left(\frac{u^2-u_x^2}{\Delta_{ex}^2 u^3} I2_x I0_y I0_z - \frac{u_x u_y}{\Delta_{ey}^2 u^3} I1_x I1_y I0_z - \frac{u_x u_z}{\Delta_{ez}^2 u^3} I1_x I0_y I1_z \right) \\
\Psi_y &= \int d^3u \left(\frac{u^2-u_y^2}{\Delta_{ey}^2 u^3} I2_y I0_z I0_x - \frac{u_y u_z}{\Delta_{ez}^2 u^3} I1_y I1_z I0_x - \frac{u_y u_x}{\Delta_{ex}^2 u^3} I1_y I0_z I1_x \right) \\
\Psi_z &= \int d^3u \left(\frac{u^2-u_z^2}{\Delta_{ez}^2 u^3} I2_z I0_x I0_y - \frac{u_z u_x}{\Delta_{ex}^2 u^3} I1_z I1_x I0_y - \frac{u_z u_y}{\Delta_{ey}^2 u^3} I1_z I0_x I1_y \right)
\end{aligned} \tag{12}$$

where, $u^2 = u_x^2 + u_y^2 + u_z^2$, $In_m = In\left(\frac{1}{2\Delta_{em}^2}, \frac{1}{2\Delta_{im}^2}, u_m\right)$ and functions In are given by:

$$\begin{aligned}
I0(a,b,c) &= \sqrt{\tfrac{\pi}{a+b}} \exp\left(-\tfrac{ab}{a+b}c^2\right) \\
I1(a,b,c) &= -I0(a,b,c) \cdot \tfrac{bc}{a+b} \\
I2(a,b,c) &= I0(a,b,c) \cdot \left[\tfrac{1}{2(a+b)} + \tfrac{b^2c^2}{(a+b)^2}\right]
\end{aligned} \tag{13}$$

The BBS for the REC cooling section is calculated according to the given equations and is used in finding the equilibrium parameters of the electron bunches, as described in Section 3.2.

5.2 Space charge tune shift

In a circularly symmetric case with Gaussian transverse density distribution of e-bunches, the equation of motion of an individual electron is:

$$r'' = K_e \frac{1}{r}\left(1 - e^{-\frac{r^2}{2\sigma_e^2}}\right) - \kappa r \tag{14}$$

where $K_e = \frac{2I_e}{I_a(\gamma\beta)^3} \approx \frac{2I_e}{I_a\gamma^3}$, $I_a \approx 17 \cdot 10^3$ A, $\sigma = \sigma_x = \sigma_y$, I_e is a bunch's peak current, and κ represents an external focusing.

Expanding Eq. (14) with respect to a small parameter r/σ we get:

$$\begin{cases} x'' = \frac{K_e}{2\sigma_e^2} x - \kappa_x x \\ y'' = \frac{K_e}{2\sigma_e^2} y - \kappa_y y \end{cases} \tag{15}$$

where $K_p = K_e I_p / I_e$.

A focusing perturbation with a gradient $k(s)$ in a circular machine leads to a tune shift:

$$\Delta\nu = \frac{1}{4\pi}\int_0^{C_R} \beta(s)k(s)ds \tag{16}$$

From Eqs. (15) and (16) we get for the tune shift induced by the space charge (SC):

$$\Delta\nu_{ex,ey} = \frac{I_e}{4\pi I_a\gamma^3}\int_0^{C_R} \frac{\beta(s)}{\sigma_e^2(s)}ds = \frac{I_e C_R}{4\pi I_a\gamma^3\varepsilon_{x,y}} \tag{17}$$

In the optimizations procedure described in Section 3.2 we used formula (17) for quick estimates of the space charge tune shift. The goal was to keep it below 0.2.

For the finalized lattice the space charge tune shift is calculated along the lattice, according to:

$$\Delta\nu_{x,y} = \frac{I_e}{2\pi I_a\gamma^3}\int_0^{C_R} \frac{\beta_{x,y}}{\sigma_{x,y}(\sigma_x+\sigma_y)} \tag{18}$$

where $\beta_{x,y}$ and $\sigma_{x,y}$ are local horizontal and vertical β-functions and transverse sizes of electron beam.

The final values for the SC-induced tune shifts are $\Delta\nu_x = \Delta\nu_y$ =0.14.

5.3 Beam-beam effect

The protons co-traveling with the electrons in the cooling section produce additional (beam-beam) focusing for the e-bunches.

From considerations similar to the ones in Section 5.2, the beam-beam parameter can be calculated as:

$$\xi_{x,y} = \frac{I_p\beta_{eCS(x,y)}L_{CS}}{2\pi I_a\gamma^3\sigma_{p(x,y)}(\sigma_{px}+\sigma_{py})} \tag{19}$$

where I_p is the proton bunch peak current, $\beta_{eCS(x,y)}$ are electrons' horizontal and vertical β-functions in the cooling section, L_CS is the CS length and $\sigma_{p(x,y)}$ are proton bunch transverse sizes in the CS.

To check whether beam-beam effect is tolerable for each set of considered parameters we were performing the tracking studies which included a realistic focusing from a proton bunch with Gaussian transverse distribution [16, 17]. The beam-beam was modeled as a focusing kick ($\delta\theta_{x,y}$) acting on an electron (displaced by x, y from the center of the proton bunch) on each pass through the cooling section:

$$\delta\theta_x = \frac{I_p L_{CS}}{I_a \gamma^3 \beta^3}\mathcal{I}_x \cdot x, \quad \delta\theta_y = \frac{I_p L_{CS}}{I_a \gamma^3 \beta^3}\mathcal{I}_y \cdot y$$
$$\mathcal{I}_x = \int_0^\infty \frac{\exp\left(-\frac{x^2}{2(\sigma_{px}^2+q)} - \frac{y^2}{2(\sigma_{py}^2+q)}\right)}{(\sigma_{px}^2+q)^{3/2}(\sigma_{py}^2+q)^{1/2}} dq \tag{20}$$
$$\mathcal{I}_x = \int_0^\infty \frac{\exp\left(-\frac{x^2}{2(\sigma_{px}^2+q)} - \frac{y^2}{2(\sigma_{py}^2+q)}\right)}{(\sigma_{px}^2+q)^{1/2}(\sigma_{py}^2+q)^{3/2}} dq$$

The studies showed that for the parameters listed in Table 1: $\xi_x = 0.04$, $\xi_y = 0.09$, the electrons' motion is stable, and the beam-beam effect neither results in the emittance growth, nor creates a noticeable halo for the electron bunches.

An additional effect of the p-e focusing results from a non-uniformity of the longitudinal distribution of a proton bunch. Because the proton bunch has a Gaussian distribution in the longitudinal direction, different slices of an e-bunch will see different focusing from protons. This unavoidable focusing mismatch can cause emittance dilution [18]. The dilution of the projected emittance can be estimated as:

$$\frac{\langle \delta\varepsilon \rangle}{\varepsilon} = 2(\pi\xi)^2 \int_{-\infty}^{\infty} f_{ze} \left(e^{-\frac{1}{2}} - e^{-\frac{z^2}{2\sigma_{zi}^2}} \right)^2 dz \tag{21}$$

Assuming $\xi < 0.1$, we get $\langle \delta\varepsilon \rangle / \varepsilon < 0.015$ for the REC parameters.

5.4 Beam lifetime

The Bremsstrahlung, Touscheck and residiual gas scattering lifetimes were calculated for the REC to determine the effect limiting the electrons lifetime.

The Bremsstrahlung lifetime was found to be of the order of 50 hours [19].

The local Touscheck loss rates were calculated for the REC lattice using optics at the end of every element. For the optimized momentum aperture (see Section 7), after integrating over the ring circumference, the lifetime was found to be 47 seconds.

Finally, the lifetime defined by the elastic scattering on the residual gas was calculated as:

$$\tau_{scatt}[\text{hours}] = 10.25 \frac{(cp)^2[\text{GeV}^2]\epsilon_A[\text{mm} \cdot \text{mrad}]}{\langle \beta[\text{m}] \rangle P[\text{nTorr}]} \tag{22}$$

where $\langle \beta \rangle$ is a β-function averaged over the ring lattice, P is the residual gas pressure and an acceptance ϵ_A determined by the dynamic aperture $A = N \cdot \sigma$ is given by

$$\epsilon_A = \frac{A^2}{\beta} = n^2\varepsilon \tag{23}$$

Assuming $P = 0.5$ nTorr and substituting REC parameters into Eqs. (22) and (23) one finds $\tau_{scatt(x)} = 16.2$ s and $\tau_{scatt(y)} = 23.2$ s for scattering in the horizontal and vertical directions respectively.

Based on the outlined considerations we assume that the electrons lifetime in the REC is 16 seconds.

5.5 Impedance and instabilities

The REC is a high-current low-energy ring. The collective instabilities in the REC require special attention. The studies of instabilities (see [20] for example) are ongoing. In a meantime, in this section we give a few estimates for the effects under consideration.

A longitudinal single bunch instability (a microwave instability) is suppressed if the ring impedance is below the threshold value, which can be roughly estimated from the Keil-Schnell-Boussard criterion:

$$\left|\frac{Z_\parallel}{n}\right| \lessapprox \sqrt{\frac{\pi}{2}} Z_0 \frac{\gamma \alpha_p \sigma_\delta^2 \sigma_z}{r_e N_e} \tag{24}$$

where $Z_0 = 377\ \Omega$ is the impedance of free space, r_e is the calssical electron radius, α_p is the REC momentum compaction, N_e is a number of electrons per bunch and σ_δ and σ_z are respectively the electron bunch's relative energy spread and rms length.

For the REC parameters the limit is 78 mΩ.

While the threshold impedance is small, it seems to be achievable. For example, from [20] it is expected from scaling scaling the NSLS-II results that for the REC the reasonable resistive wall impedance is $\left|\frac{Z_\parallel}{n}\right|_{RW} \approx 47$ mΩ.

A somewhat smaller resistive wall impedance is estimated in [21] from:

$$\left|\frac{Z_\parallel}{n}\right|_{RW} = (1-i)\frac{\sigma_z}{r_{ch}\sigma_{con}\delta_{skin}} \tag{25}$$

where $r_{ch} = 30$ mm is the radius of vacuum chamber, $\sigma_{con} \approx 5.96 \cdot 10^7$ $(\Omega \cdot m)^{-1}$ is Cu conductivity, and $\delta_{skin} \approx 3$ μm is the skin depth at 0.5 GHz corresponding the e-bunch length. For the current REC parameters the resistive wall impedance is ≈ 25 mΩ.

Besides resistive wall impedance, the coherent synchrotron radiation (CSR) is also important for the longitudinal instability in an electron storage ring. Since the REC contains a long wiggler section,

the CSR impedance there can be significant, and the highest frequencies for the electron bunch, might become unstable. The remedy for such a problem is smoothly varying the gap in the wiggler, thus reducing the impedance [20].

One can estimate the threshold for the transverse mode-coupling instability similar to [21]. For the latest REC parameters the threshold is $Z_{\perp}^{thr} \approx 5$ kΩ/m.

The transverse resistive wall impedance can be calculated from the Panofsky-Wenzel theorem:

$$Z_{\perp}^{RW} = \frac{C_R}{\pi r_{ch}^2} \left| \frac{Z_{\parallel}}{n} \right|_{RW} \tag{26}$$

Substituting the optimized REC parameters into Eq. (26), we get $Z_{\perp}^{RW} \approx 3.77$ kΩ/m, which is below the instability threshold.

A detailed study of the instabilities is left for future work, but so far, all REC parameters look feasible.

6 Summary

In this manuscript we presented a brief description of the status of the design efforts for the Ring Electron Cooler capable of providing the cooling required for the EIC operation at the top energy.

Careful optimization of the REC parameters allowed us to maintain the required cooling times while reducing the bunch charge and average current in the ring by a factor of 2.3 and reducing the e-bunch peak current by a factor of 2.7 (utilization of flat-top electron bunches provided additional improvement to the peak current).

Various collective effects including IBS, beam-beam scattering in the cooling section and beam-beam space charge focusing are taken into account in the REC optimizations.

The realistic lattice for the REC compatible with the EIC Low Energy Cooler was fully developed. Lattice optimization provided the dynamic aperture of 10σ and momentum aperture of 0.5%.

The damping wigglers with realistic fields and optimized chromaticity contribution were developed. The wigglers are the integral part of the current REC lattice and their field nonlinearities are included in all beam-dynamics studies.

Parameters of a dual RF system providing required electron bunch profile were calculated.

The conceptual design of the REC injection section was developed. The factors limiting the beam lifetime were considered and a feasible injection scheme providing required average e-bunch charge was devised.

The studies of tolerances to magnets misalignments and tolerances to errors in various REC subsystems (RF, injection, diagnostic) based on cooling requirements are successfully going.

There are several areas which require additional studies.

Systematic studies of instabilities must be performed (coherent wiggler instability, transverse mode-coupling instability, transverse and longitudinal coupled-bunch instability, electron-ion instability etc.)

Beam loading in the RF and its effects on longitudinal bunch distribution need to be studied.

Feedbacks (both to keep e-beam quality in the cooling section and to counteract possible instabilities) have to be considered.

Various engineering systems (diagnostic, vacuum, machine protection) must be devised.

Operating the REC at lower energies must be considered.

These studies are required to bring the REC to the next design stage.

The present conceptual design efforts showed no showstoppers. The REC parameters were found to be feasible.

References

[1] G. I. Budker, An effective method of damping particle oscillations in proton and antiproton storage rings, At. Energ. 22, 346 (1967) [Sov. At. Energy 22, 438 (1967)].

[2] G. I. Budker et al., Experimental study of electron cooling, Part. Accel. 7, 197 (1976).

[3] S. Seletskiy et al., Accurate setting of electron energy for demonstration of first hadron beam cooling with RF accelerated electron bunches, Phys. Rev. Accel. Beams 21, 111004 (2019).

[4] A. Fedotov et al., Experimental demonstration of hadron beam cooling using radio frequency accelerated electron bunches , Phys. Rev. Lett. 124, 084801 (2020).

[5] D. Kayran et al., High brightness electron beams for linac based bunched beam electron cooling, Phys. Rev. Accel. Beams 23, 021003 (2020).

[6] X. Gu et al., Stable operation of a high voltage high current dc photoemission gun for the bunched beam electron cooler in RHIC, Phys. Rev. Accel. Beams 23, 013401 (2020).

[7] H. Zhao et al., Cooling simulation and experimental benchmarking for an RF based electron cooler, Phys. Rev. Accel. Beams 23, 074201 (2020).

[8] S. Seletskiy et al., Obtaining transverse cooling with non magnetized electron beam, Phys. Rev. Accel. Beams 23, 110101 (2020).

[9] S. Seletskiy, Redistribution of cooling rates for electron bunch with nonuniform density, BNL-223860-2023-TECH (2023).

[10] S. Seletskiy, Redistribution of cooling rates in non-magnetized electron coolers, unpublished.

[11] J. D. Bjorken and S. K. Mtingwa, Intrabeam scattering, Part. Accel. 13, 115 (1982).

[12] S. Nagaitsev, Intrabeam scattering formulas for fast numerical evaluation, Phys.Rev. STAccel.Beams 8, 064403 (2005).

[13] H. Zhao, M. Blaskiewicz, Electron Heating by Ions in Cooling Rings, TUPLM24, NAPAC2019, Lansing, MI, USA (2019).

[14] S. Seletskiy et al., Optical properties of wigglers for EIC Ring Electron Cooler, BNL-225896-2024-TECH (2024).

[15] Private communications with O. Tchoubar.

[16] S. Seletskiy, A.V. Fedotov, D. Kayran, J. Kewisch, Proton-electron focusing in EIC Ring Electron Cooler, WEPA78, NA-PAC2022, Albuquerque, NM, USA (2022).

[17] S. Seletskiy, Beam-beam effects in EIC electron coolers, ICFA workshop: Beam-Beam Effects in Circular Colliders BB24, September 2-5, 2024. (`https://indico.global/event/9305/contributions/90682/attachments/41498/77715/eCoolBeamBeam.pdf`)

[18] S. Seletskiy, S. Nagaitsev, Focusing effect of proton bunch with Gaussian longitudinal distribution on electrons in EIC Ring Cooler, BNL-224133-2023-TECH (2023).

[19] Private communications with B. Podobedov.

[20] Blednykh et al., Microwave instability threshold from coherent wiggler radiation impedance in storage rings, Phys. Rev. Accel. Beams 26, 051002 (2023).

[21] He. et al. Ring-based electron cooler for high energy beam cooling, Phys. Rev. Accel. Beams 24, 043501 (2021).